Neurobiology of Disease 111 (2018) 91–101

Contents lists available at ScienceDirect

Neurobiology of Disease

journal homepage: www.elsevier.com/locate/ynbdi

A mouse model of *DEPDC5*-related epilepsy: Neuronal loss of *Depdc5* causes dysplastic and ectopic neurons, increased mTOR signaling, and seizure susceptibility

Christopher J. Yuskaitis[a,b,c], Brandon M. Jones[a], Rachel L. Wolfson[d], Chloe E. Super[a], Sameer C. Dhamne[a], Alexander Rotenberg[a,b,c,i], David M. Sabatini[d,e,f,g,h], Mustafa Sahin[a,c,*,1], Annapurna Poduri[a,b,c,*,1]

[a] Department of Neurology, F.M. Kirby Neurobiology Center, Boston Children's Hospital, Boston, MA 02115, USA
[b] Division of Epilepsy and Clinical Neurophysiology and Epilepsy Genetics Program, Boston Children's Hospital, Boston, MA 02115, USA
[c] Department of Neurology, Harvard Medical School, Boston, MA 02115, USA
[d] Whitehead Institute for Biomedical Research, 455 Main Street, Cambridge, MA 02142, USA
[e] Department of Biology, Massachusetts Institute of Technology, 77 Massachusetts Avenue, Cambridge, MA 02139, USA
[f] Howard Hughes Medical Institute, Department of Biology, Massachusetts Institute of Technology, 77 Massachusetts Avenue, Cambridge, MA 02139, USA
[g] Koch Institute for Integrative Cancer Research at MIT, 77 Massachusetts Avenue, Cambridge, MA 02139, USA
[h] Broad Institute, 415 Main Street, Cambridge, MA 02142, USA
[i] Neuromodulation Program, Department of Neurology, Boston Children's Hospital, Harvard Medical School, Boston, MA 02115, USA

ARTICLE INFO

Keywords:
DEPDC5
Focal cortical dysplasia
mTOR
Familial focal epilepsy
Seizures
Conditional knockout
Megalencephaly

ABSTRACT

DEPDC5 is a newly identified epilepsy-related gene implicated in focal epilepsy, brain malformations, and Sudden Unexplained Death in Epilepsy (SUDEP). *In vitro*, DEPDC5 negatively regulates amino acid sensing by the mTOR complex 1 (mTORC1) pathway, but the role of DEPDC5 in neurodevelopment and epilepsy has not been described. No animal model of *DEPDC5*-related epilepsy has recapitulated the neurological phenotypes seen in patients, and germline knockout rodent models are embryonic lethal. Here, we establish a neuron-specific *Depdc5* conditional knockout mouse by cre-recombination under the *Synapsin1* promotor. $Depdc5^{flox/flox}$-$Syn1^{Cre}$ (*Depdc5*cc+) mice survive to adulthood with a progressive neurologic phenotype that includes motor abnormalities (*i.e.*, hind limb clasping) and reduced survival compared to littermate control mice. *Depdc5*cc+ mice have larger brains with increased cortical neuron size and dysplastic neurons throughout the cortex, comparable to the abnormal neurons seen in human focal cortical dysplasia specimens. *Depdc5* results in constitutive mTORC1 hyperactivation exclusively in neurons as measured by the increased phosphorylation of the downstream ribosomal protein S6. Despite a lack of increased mTORC1 signaling within astrocytes, *Depdc5*cc+ brains show reactive astrogliosis. We observed two *Depdc5*cc+ mice to have spontaneous seizures, including a terminal seizure. We demonstrate that as a group *Depdc5*cc+ mice have lowered seizure thresholds, as evidenced by decreased latency to seizures after chemoconvulsant injection and increased mortality from pentylenetetrazole-induced seizures. In summary, our neuron-specific *Depdc5* knockout mouse model recapitulates clinical, pathological, and biochemical features of human *DEPDC5*-related epilepsy and brain malformations. We thereby present an important model in which to study targeted therapeutic strategies for *DEPDC5*-related conditions.

1. Introduction

DEPDC5 is a gene that has been recently associated with familial focal epilepsy as well as sporadic epilepsy (Dibbens et al., 2013; Epi4K and Epilepsy Phenome/Genome, 2017; Ishida et al., 2013; Lal et al., 2014; Picard et al., 2014). The list of epilepsy syndromes associated with pathogenic variants in *DEPDC5* is expanding, with the severe early onset epilepsy syndrome known as infantile spasms recently included (Carvill et al., 2015). *DEPDC5* variants may also confer an increased risk for Sudden Unexplained Death in Epilepsy (SUDEP) (Bagnall et al., 2016; Nascimento et al., 2015). In addition to a role in non-lesional focal epilepsy, *DEPDC5* has also been associated with epileptogenic

* Corresponding authors at: Department of Neurology, F.M. Kirby Neurobiology Center, Boston Children's Hospital, Boston, MA 02115, USA.
E-mail addresses: Mustafa.Sahin@childrens.harvard.edu (M. Sahin), Annapurna.Poduri@childrens.harvard.edu (A. Poduri).
[1] Equal contributions.

https://doi.org/10.1016/j.nbd.2017.12.010
Received 5 October 2017; Received in revised form 27 November 2017; Accepted 19 December 2017
Available online 20 December 2017

structural brain malformations, from focal cortical dysplasia (FCD) (Baulac et al., 2015; D'Gama et al., 2015a; Scheffer et al., 2014) to large cortical malformations, such as hemimegalencephaly (D'Gama et al., 2015b; Ricos et al., 2016; Scerri et al., 2015). Pathological examination of resected human brain tissue from patients with pathogenic variants in *DEPDC5* reveals dysplastic neurons and evidence of mTOR pathway disruption (Scerri et al., 2015).

Altered mTOR complex 1 (mTORC1) signaling is implicated in many neurologic conditions including epilepsy, brain malformations, and autism (Lipton and Sahin, 2014). At the cellular level, the mTORC1 pathway is activated by pro-growth factors such as neurotrophins, growth factors, and amino acids, and inhibited by metabolic stress such as nutrient starvation and endoplasmic reticulum stress. The product of *DEPDC5*, pleckstrin (DEP) domain-containing protein 5 (DEPDC5) is a key member of the amino acid sensing machinery and negatively regulates the mTORC1 pathway (Bar-Peled et al., 2013). DEPDC5 is ubiquitously expressed in the developing and adult brain, with high levels of expression in neurons (Dibbens et al., 2013).

DEPDC5 is a component of the GATOR1 complex along with NPRL2 and NPRL3. Collectively, the GATOR1 complex inhibits RagA/B- and RagC/D-mediated mTORC1 recruitment to lysosomal membranes and inhibits downstream mTORC1-mediated phosphorylation of S6 kinase and its substrate S6 (Saxton and Sabatini, 2017; Wolfson et al., 2017). The GATOR1 complex is a key regulator of cellular amino acid and nutrient detection in non-neuronal cell lines. These signaling pathways are unique to the GATOR complex and function independently of TSC1/TSC2 signaling (Shimobayashi and Hall, 2016). Given the relatively recent recognition of their role in epilepsy and brain development, the role of *DEPDC5* and GATOR1 signaling in neuronal function remains largely unexplored.

Recently, Baulac and colleagues demonstrated a post-zygotic, somatic mutation of *DEPDC5* in the brain lesion of a patient with a germline *DEPDC5* mutation (Baulac et al., 2015). This provides evidence that a "two-hit" functional knockout of *DEPDC5* may underlie brain malformations in some patients, particularly those with MRI-evident brain lesions (Scheffer et al., 2014). No animal model of *DEPDC5*-related epilepsy exists, and many animal models of GATOR1 complex genes are embryonic lethal, including a *Depdc5*$^{-/-}$ mouse (Dickinson et al., 2016). A *Depdc5*$^{-/-}$ rat model is embryonic lethal, and the *Depdc5*$^{+/-}$ rats do not display spontaneous seizures and seizure thresholds were not evaluated (Marsan et al., 2016). Animal models of other mTOR pathway regulators are lethal in the embryonic period, including *Tsc1* and *Tsc2* (Han and Sahin, 2011) and *Pten* (Di Cristofano et al., 1998). The synapsin promoter driving Cre-recombinase expression starting at embryonic day 12–13 has been successfully utilized to generate neuron-specific inactivation models of other mTORopathies (Meikle et al., 2007; Yuan et al., 2012; Zhu et al., 2001).

Here, we report the generation and characterization of a neuron-specific *Depdc5* mouse model, *Depdc5*$^{flox/flox}$-*Syn1*^{Cre} (*Depdc5*cc+), which displays a larger brain size, early mortality, lowered seizure threshold, evidence of mTOR hyperactivation, ectopic neurons in the hippocampus, and dysplastic neurons in the cortex. Taken together, we present the first mammalian model that recapitulates many features of the human conditions associated with pathogenic variants in *DEPDC5*.

2. Methods

2.1. Mouse alleles, breeding strategy, and phenotyping

Mouse experiments were performed in a mixed-strain background using equal numbers of male and female mice. All mice were housed in a 12-h light-dark cycle, climate controlled room, with access to food and water *ad lib*. *Depdc5*$^{tm1c(EUCOMM)Hmgu}$ conditional mice (referred to as *Depdc5*$^{c/c}$) contain loxP sites flanking exon 5 of the *Depdc5* gene. Germline loss of *Depdc5* exon 5 results in embryonic lethality (Dickinson et al., 2016). To generate the neuron-specific *Depdc5* conditional knockout mice, the homozygous *Depdc5* conditional mice (*Depdc5*$^{c/c}$) were bred with female neuron-specific synapsin I cre (*SynI—Cre*) allele mice from our existing colony (Yuan et al., 2012). *Depdc5*$^{c/w}$-*SynICre* (*Depdc5*$^{c/w+}$) females were bred with *Depdc5*$^{c/c}$ male mice to generate litters of homozygous neuronal knockout *Depdc5*$^{c/c}$-*SynCre*$^{+}$ (referred to herein as *Depdc5*cc+), heterozygous *Depdc5*$^{c/w}$-*SynCre*$^{+}$ (referred to herein as *Depdc5*cw+), and littermate control *Depdc5*$^{c/w}$-*SynCre*$^{-}$ and *Depdc5*$^{c/c}$-*SynCre*$^{-}$ mice. Mice were monitored daily for survival and weighed at weaning, 30 days, 60–75 days, and 90 days of age.14 days, 28 days, 60 days and 90 days. During routine handling, animals were monitored for spontaneous convulsive seizures by visual inspection. Phenotypic evaluation for hunchback posture, Straub tail positioning, and tremors was performed as previously described (Yuan et al., 2012). As a test of progressive neurology dysfunction, hind limb strain test was applied to mice > 90 day old, and scored as follows: 1, normal lateral spread of hind limbs; 2, hind limb shaking and out-of-plane movement; 3, hind limb movement toward midline; 4, clasping of hind limbs. At time of sacrifice, body weights and dissected brain weights (without olfactory bulbs) were recorded. All mouse procedures were performed in accordance with the Guide for the Humane Use and Care of Laboratory Animals, and the study was approved by the Animal Care and Use Committee of Boston Children's Hospital.

2.2. DNA analysis

DNA was prepared from mouse toes/tails by standard procedures. Genotyping at the *Depdc5* gene was performed using a primer pair that allows simultaneous analysis of both conditional and wild-type alleles (forward: 5′-CATAGACATCTTGATAAGGTCTTAGCC-3′ and reverse: 5′-TCAAGTGCAAGATCTTAAGTGATTGGC-3′), followed by agarose gel electrophoresis. An 852 base pair (bp) band was detected for the wild-type allele, and a 1069 bp band was detected for the conditional allele with the flanking loxP sites. Primers that amplify a 300 bp portion of the *Cre* recombinase were used to assess the presence of the *SynI-Cre* allele (Zhu et al., 2001).

2.3. RT-PCR analysis

RNA was extracted from adult mouse cortical and liver samples using a RNEasy Mini Kit (Qiagen). We used 1 μg of each RNA sample for reverse transcription with the iScript cDNA synthesis kit (Biogen). Quantitative PCR was performed using iScript Reverse Transcriptase Supermix (Biogen) on an Applied Biosystems 7300 Real-Time PCR System (Life Technologies). *Depdc5* expression was normalized to *Gapdh* and expressed as a relative quantity. Parallel reactions containing no reverse transcriptase were used as negative controls to confirm the removal of all genomic DNA. The oligonucleotide sequences of the primers used are as follow: primer set 1 for *Depdc5* forward GTGTGGACCAGACTGTGACTC and reverse GCACAGGTGCTC ACCAAACTT, primer set 2 for *Depdc5* forward CCCCAATGATGAGTAC AGTCCTT and reverse CCACCAGGTCAAGAGTCACA, and *Gapdh* forward TGCGACTTCAACAGCAACTC and reverse ATGTAGGCCATGAGG TCCAC. RT-PCR product from *Depdc5* primer set 2 was run on an acrylamide gel to evaluate product size. Results were estimated as cycle threshold (Ct) values; the Ct was calculated as the mean Ct for the target gene minus the mean Ct for the control gene. The fold differential expression in the target gene of KO compared with control cortical tissue was expressed as $2^{-\Delta\Delta Ct}$. Data analysis and graphics were performed using GraphPad Prism 5 software and represent the results of 5 mice per group for cortex and 3 mice per group for liver. Each sample was run in triplicate for each gene.

2.4. Immunohistochemistry

Coronal brain sections of 87–111 day-old adult mice were collected, fixed, and vibrotome-sectioned at 35 μm using standard methods. Floating sections were immunolabeled using the following primary

antibodies: mouse anti-NeuN (AB_2298772), mouse anti-GFAP (AB_561049), rabbit-phospho-S6 Ribosomal Protein (Ser 240/244) (AB_10694233), rabbit-DEPDC5 (AB_2010354; AB_2010353); SMI-311 (AB_2565383). Primary antibodies were detected with the following secondary antibodies: goat anti-mouse 488 (AB_2534069), goat anti-rabbit 555 (AB_2535849). Nuclei were stained with Hoescht 33342 (ThermoFisher). Images were acquired using a Zeiss LSM700 Laser Scanning Confocal Microscope equipped with Plan Apochromat × 10/0.3 and × 25/0.8 objectives. Neuronal density was analyzed by counting on average 100 NeuN-positive nuclei in each cortical layer per animal using Optical Fractionator in StereoInvestigator (MBF Bioscience). The remainder of images were analyzed using the ImageJ software. Blinded cortical thickness measurements were taken a minimum of 6 locations per section. Area measurements of Layer V NeuN-positive neurons were performed from at least 25 cells per section. A minimum of 3 anatomically match sections per animal were used from three control mice and four *Depdc5*cc+ mice. Data are expressed as mean ± S.E.M.

2.5. Western blotting

To evaluate protein levels, protein extracts were prepared from dissected cortical tissue of adult control and Depdc5cc+ mice between 92 and 122 days old. Western blotting was performed using similar amounts of protein extract per lane in 8–12% SDS polyacrylamide precast gels (BIO-RAD Laboratories). Western blots were done using the following primary antibodies: mouse anti-GFAP (AB_561049), rabbit-phospho-S6 Ribosomal Protein (Ser 240/244) (AB_10694233), mouse-Ribosomal Protein S6 (AB_1129205), mouse-TSC1 (AB_2533292), rabbit-TSC2 (AB_10547134), rabbit-AKT (AB_329827), rabbit-phospho-AKT(Ser473) (AB_2315049), rabbit-DEPDC5 (AB_2010354; AB_2010353); mouse-alpha-tubulin (AB_2688039). IRDye 800CW- or 680LT-conjugated secondary antibodies (1:1500; LI-COR) were used. To visualize bands, Odyssey Fc Imager was used and densitometry analysis was performed using Image Studio Software (LI-COR). Each band was normalized to the alpha-tubulin signal per sample.

2.6. EEG telemetry and PTZ-induced seizure threshold

EEG recording was performed as previously described with implanted wireless telemetry transmitters (PhysioTel ETA-F10; DSI, Data Sciences International) (Dhamne et al., 2017). One-channel video-EEG was recorded differentially between the reference (right olfactory bulb) and active (left occipital lobe) electrodes, with data collected over 3–14 days, which included day and night cycles. The EEG was sampled at 1000 Hz. Prior to implanted electrodes, all mice were also monitored in their home cages by direct observation for at least 1 h per week throughout development for evidence of spontaneous convulsive seizures, in addition to reviewing the video-EEG data. At the end of the recording period, animals were challenged to exposed to proconvulsant to evaluate seizure threshold: adult *Depdc5*cc+ and littermate control mice were challenged with a convulsive dose (40 mg/kg; intraperitoneally, i.p.) of pentylenetetrazole (PTZ; Sigma-Aldrich, Co), a $GABA_A$ receptor antagonist (Dhamne et al., 2015; Dhamne et al., 2017). Latency to generalized tonic-clonic seizures (GTCs), number of seizures and, total duration of GTCs were recorded per mouse; animals without seizures were assigned a time of 20 min at the end of the PTZ challenge observation period.

2.7. EEG analysis

The first 24 h of recording were considered an acclimation period, and data from this period were not analyzed. Video-EEGs were reviewed offline for behavioral or electrographic seizures. A 1 h segment of daytime (between 11 am and 3 pm) and a 1 h nighttime (between 11 pm – 3 am) baseline EEG was analyzed for epileptiform spikes and spectral power band analysis. An epileptiform discharge was defined as a run of continuous spikes ≥ 5 s in duration on the EEG (Dhamne et al., 2017). Power in frequency bands of the baseline EEG was calculated by transforming the raw EEG signal to frequency domain using the fast Fourier transform (FFT) technique. The power frequency bands were analyzed as a ratio of its absolute power to the total absolute power (1–80 Hz), to compensate for inter-subject variability and artifacts.

2.8. Statistical analysis

Statistical analysis was performed by GraphPad Prism 7 software. The results are presented as mean ± SEM. Normality was assessed by Kolmogorov–Smirnov normality test. Comparisons between two groups were performed by unpaired two-tailed Student's *t*-test for parametric data and by Mann–Whitney test for non-parametric data. Comparisons between multiple groups were performed by 1-way ANOVA with Tukey's multiple comparison test as post-hoc analysis for parametric data and by a Kruskal–Wallis test for non-parametric data. A log-rank (Mantel-Cox) test was performed to compare the Kaplan–Meier analysis for mortality and seizure latency.

3. Results

3.1. Conditional neuron-specific Depdc5 knockout mice survive to adulthood

We generated a conditional neuron-specific *Depdc5* knockout mouse model to evaluate DEPDC5 function in the brain *in vivo*. *Depdc5*$^{c/c}$ mice contain loxP sites flanking exon 5 of the *Depdc5* gene and are embryonic lethal when Cre is constitutively expressed (Dickinson et al., 2016). We crossed *Depdc5*$^{c/c}$ mice with a line containing the *SynapsinI* promoter-driven cre recombinase allele (*SynICre*) that leads to recombination of loxP sites in neurons beginning at E12.5 (Zhu et al., 2001). We generated litters of conditional neuron-specific *Depdc5* knockouts (*Depdc5*cc+), heterozygous (*Depdc5*cw+), and littermate controls (*Depdc5*cc–, *Depdc5*cw–) in Mendelian ratios (Table 1).

PCR amplification of DNA isolated from tails and brains of *Depdc5*cc+ and control mice were performed to evaluate for specificity of Cre-mediated recombination. We confirmed that Cre recombination resulted in truncation of the *Depdc5* PCR product only in brain tissue of *Depdc5*cc+ mice (Fig. 1A). No reliable antibodies against mouse DEPDC5 exist currently. Although sequence homology with human DEPDC5 is 96%, several antibodies against human DEPDC5 did not reliably detect DEPDC5 in control mouse tissue by immunofluorescence or immunoblotting (data not shown). To address if the truncated *Depdc5* gene resulted in a reduction in mRNA transcript, we evaluated *Depdc5* mRNA transcripts from cortical samples of *Depdc5*cc+ mice and controls by RT-PCR. *Depdc5* mRNA from *Depdc5*cc+ cortex was 33% of littermate control levels and truncated in length, while liver samples were unchanged across the genotypes (Fig. 1B). A complete loss would not be expected in whole cortex tissue since recombination is restricted to neurons, as previously shown (Zhu et al., 2001). Together these results

Table 1
Litters of conditional neuron-specific *Depdc5* knockout mice survive in expected Mendelian ratios. Percentage (number of pups) are shown for each genotype for the 5 litters of crosses between homozygous *Depdc5* conditional (*Depdc5*$^{c/c}$) males and female *Depdc5*$^{c/w}$-*SynICre* (*Depdc5*$^{c/w+}$) mice.

Litters	*Depdc5*cc+ (KO)	*Depdc5*cw+ (Het)	*Depdc5*cc- (Ctl)	*Depdc5*cw- (Ctl)	Total
1	11% (1)	33% (3)	22% (2)	22% (2)	9
2	33% (3)	22% (2)	11% (1)	33% (3)	9
3	27% (3)	36% (4)	18% (2)	18% (2)	11
4	40% (4)	20% (2)	20% (2)	20% (2)	10
5	22% (2)	22% (2)	22% (2)	33% (3)	9
Total	27%	27%	19%	25%	48

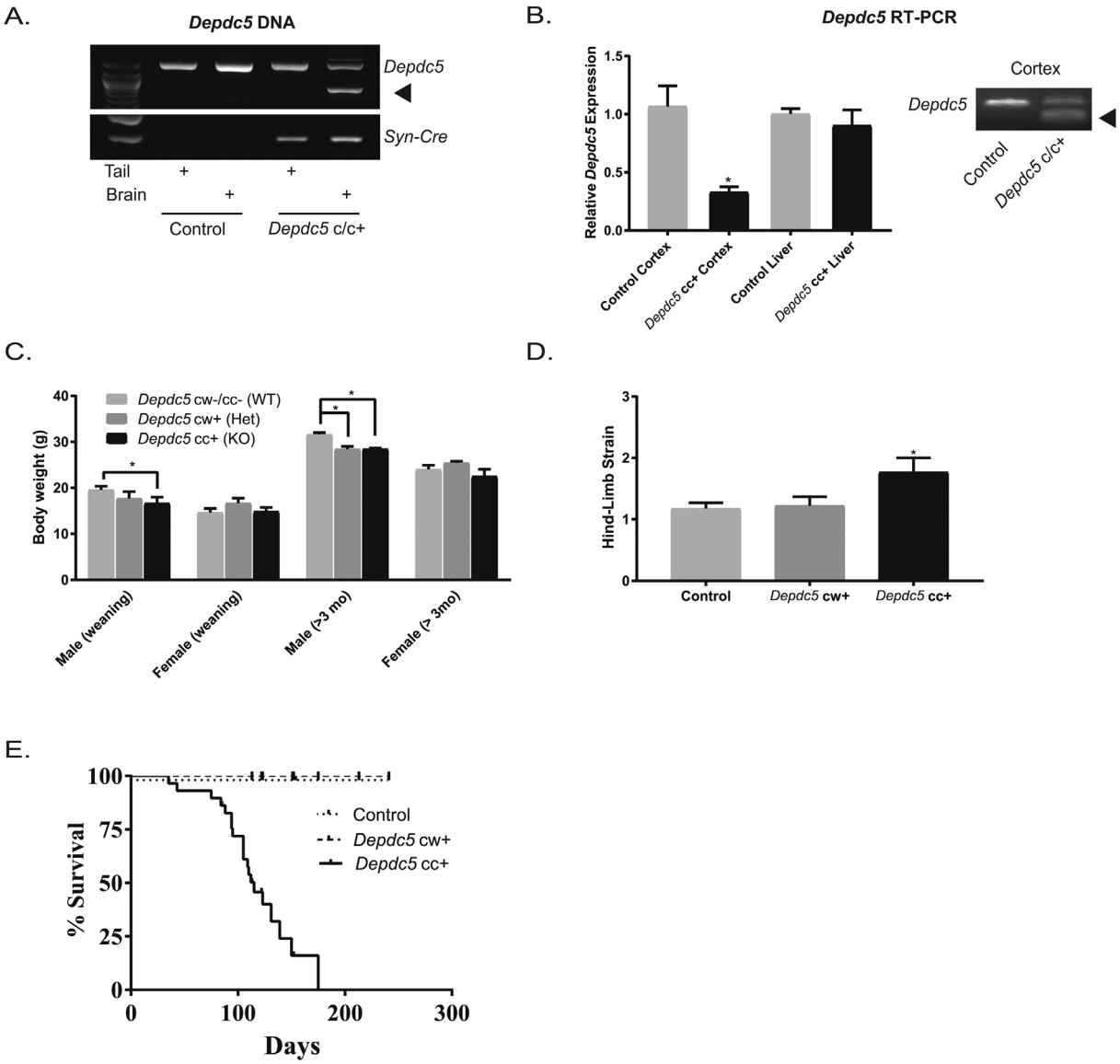

Fig. 1. Conditional neuron-specific *Depdc5* knockout (*Depdc5*cc+) mice have minimal weight loss but evidence of a progressive neurologic phenotype and reduced survival. (A) *Depdc5* PCR product is truncated (arrow) in brain tissue from $Depdc5^{f/f}$ mice with a copy of the Syn-Cre allele (*Depdc5*cc+), but not from tail or control mice samples. (B) Left: Quantitative analysis of RT-PCR of *Depdc5* transcript is reduced in *Depdc5*cc+ cortical tissue (0.33 ± 0.04; $p = 0.002$) but not liver tissue (0.90 ± 0.13) compared to controls (cortex 1 ± 0.18; liver 1 ± 0.05). Right: Gel from *Depdc5* RT-PCR product with a truncated product (arrow) only in *Depdc5*cc+ cortical tissue homogenate. (C) Compared to littermate controls, *Depdc5*cc + male mice had reduced body weight in weanlings, P21–30, (1 ± 1.3 g reduction; $p = 0.04$) and aged mice (3.1 ± 1.2 g reduction; $p = 0.03$), whereas *Depdc5*cw+ males showed a significant weight reduction only in aged mice (3.2 ± 1.3 g reduction; $p = 0.046$). No differences in female mice or between *Depdc5*cc+ and *Depdc5*cw+ were seen, $n > 6$ per sex within each genotype. (D) As a test of neurologic dysfunction, aged, > 90 days old, *Depdc5*cc+ mice had evidence of hind limb strain ($n = 13$; score = 1.8 ± 0.2) unlike control ($n = 17$; score = 1.18 ± 0.1) and *Depdc5*cw+ ($n = 9$; score = 1.22 ± 0.15) mice. (E) Monitoring survival of littermate mice revealed a markedly shortened lifespan of *Depdc5*cc+ ($n = 29$; median survival = 115 days) compared to *Depdc5*cw+ ($n = 25$) and control ($n = 30$) mice. Error bars represent mean ± SEM. *$p < 0.05$ (2-way ANOVA and Tukey's multiple comparison test).

demonstrate the neuron-specific *SynICre* expression in *Depdc5*cc+ mice leads to a truncation of the *Depdc5* gene and loss of full-length *Depdc5* transcript.

Unlike the constitutive *Depdc5* knockout mice, which are embryonic lethal, *Depdc5*cc+ and heterozygous *Depdc5*cw+ mice were viable and indistinguishable from littermate controls with exception of a mild reduction in weight gain (Fig. 1C). A reduction in weight of male *Depdc5*cc+ was evident at time of weaning and persisted through adulthood, whereas a reduction in weight of *Depdc5*cw+ mice compared to littermate controls only became evident after 3 months of age. There was no difference in the weight of female mice at any age. Subsequent experiments used equal numbers of males and females within groups, and groups with odd numbers used an extra female to decrease the effect of weight-loss in the male knockout mice. Unlike the constitutive *Depdc5* knockout mice, *Depdc5*cc+ mice do not exhibit a hunchback phenotype at any age; however, *Depdc5*cc+ mice over 60 days old demonstrate evidence of neurologic dysfunction by limb-clasping behavior (hind limb strain) compared to *Depdc5*cw+ and littermate controls (Fig. 1D). This finding was equally distributed between both male and female *Depdc5*cc+ mice.

3.2. Conditional neuron-specific Depdc5 knockout mice exhibit mortality in adulthood

Despite a lack of systemic illness or overt signs of neurologic deficit, *Depdc5*cc+ have decreased survival (median 115 days) with no mice surviving past 175 days. Littermate control and *Depdc5*cw+ mice have normal survival (Fig. 1E). *Depdc5*cc+ mice were often found dead <

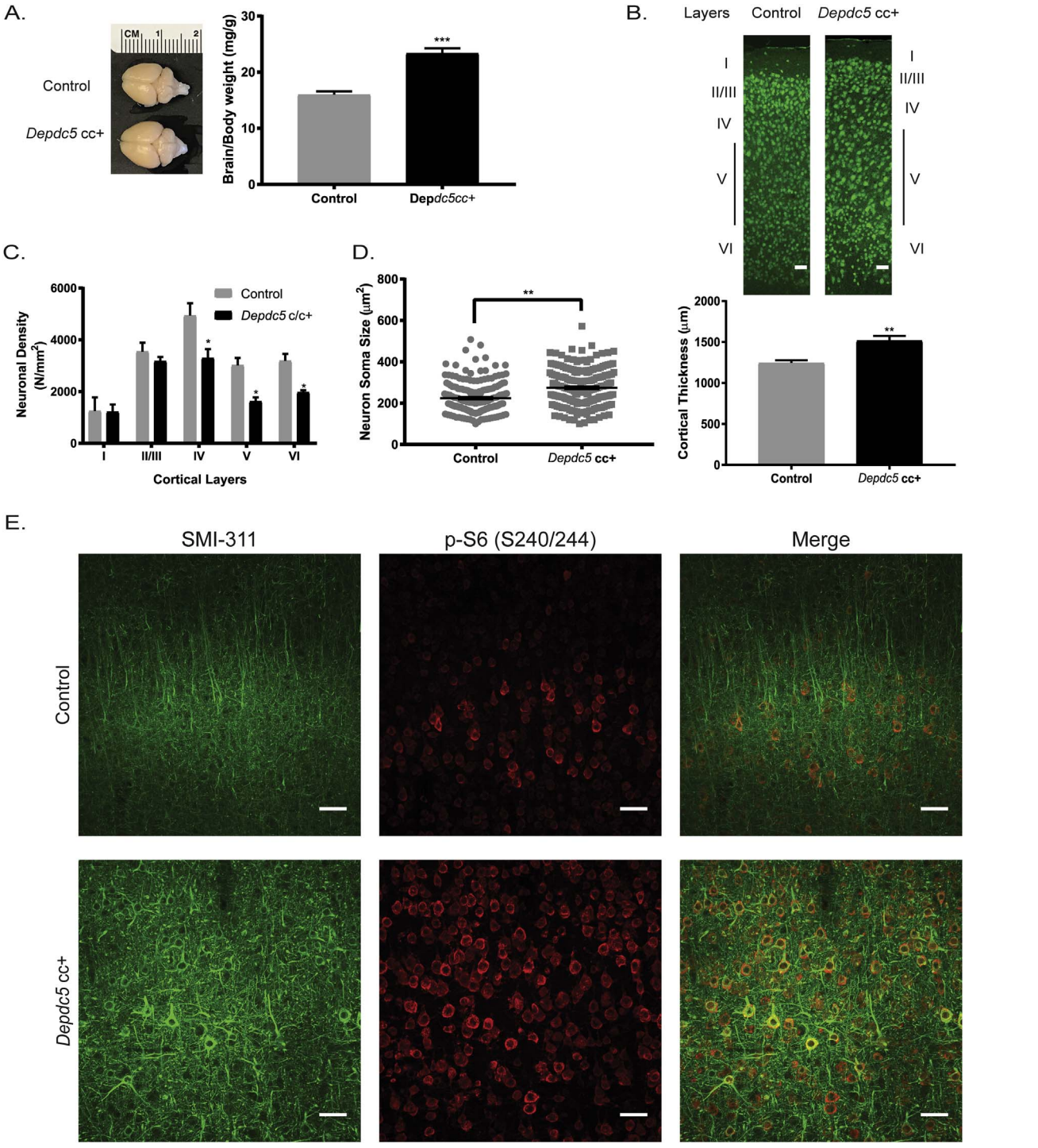

Fig. 2. Neuropathological defects in conditional neuron-specific *Depdc5* knockout (*Depdc5*cc+) mice. (A) Left: Representative images of adult dissected brains show increased brain size of *Depdc5*cc+ compared to littermate controls. Right: Brain weight is increased in *Depdc5*cc+ ($n = 10$) mice compared to littermate control (n = 13) adult > 60 day old mice. (B) Increased cortical thickness with less distinct layers in *Depdc5*cc+ adult cortex compared to littermate controls. Top: Representative NeuN stained coronal sections, scale bars: 100 μm. Bottom: Cortical thickness measurements at 6 paired sites in at least 3 sections per brain. (C) Neuronal density was unchanged in layers I-III and decreased in layers IV-V in *Depdc5*cc+ mice compared to matched controls; measured from on average 100 NeuN + neurons per layer in each animal. (D) Neuron soma size is larger in *Depdc5*cc+ layers IV-V of M1 region of cortex compared to controls, measured from at least 175 NeuN-positive neurons per genotype. (E) Dysplastic neurons within *Depdc5*cc+ brains are evident by SMI 311 staining. Top panels in control mouse cortex with linear SMI 311 staining and minimal pS6 staining. Bottom panels in *Depdc5*cc+ cortex with strong, disorganized SMI 311 staining colocalizes with pS6 staining. Scale bars: 50 μm. Sections from $n = 4$ *Depdc5*cc+ and $n = 3$ control brains. Graph error bars represent mean ± SEM. $^{*}p < 0.05$; $^{**}p < 0.01$; $^{***}p < 0.001$ (Student's *t*-test).

24 h after being observed to be normal. There was no sex difference in age of death. No wounds or major pathology was seen on the animals to explain sudden death.

During normal handling circumstances, we observed spontaneous seizures in three mice, including one *Depdc5*cc+ mouse that died at 105 days of age during a generalized tonic-clonic seizure at the time of cage changing. Another two *Depdc5*cc+ mice exhibited tonic seizures, characterized by freezing (abrupt activity arrest) with arching of the tail

and lack of response to stimulation that lasted approximately 1 min before returning to baseline; both mice died within 2 weeks of the witnessed seizure, at 100 and 123 days of age.

3.3. Neuropathological effects in Depdc5cc+ mice

We assessed the neuropathological effects of the reduction of *Depdc5* in the *Depdc5*cc+ mice. In adult mice, the *Depdc5*cc+ brains were markedly larger than littermate controls on gross inspection (Fig. 2A). After controlling for body weight, *Depdc5*cc+ brains weights were significantly greater than littermate controls after 60 days of age ($p < 0.05$) but not prior to 30 days of age ($p = 0.46$) (Fig. 2A). Analysis of sectioned brains, revealed an increase in cortical thickness in *Depdc5*cc+ mice compared to littermate controls (Fig. 2B). Neuronal density was not increased in *Depdc5*cc+ mice, but rather deeper layers had a decrease in neuronal density ($p < 0.05$) (Fig. 2C). In the deeper layers, neuronal enlargement was most evident in layer V neurons. To quantify the neuronal enlargement, blinded measurements of neuronal soma area was performed on NeuN-positive neurons in layer V of the motor cortex, as previously described (Meikle et al., 2008). We confirmed that neurons in *Depdc5*cc+ mice are significantly larger than littermate controls ($p < 0.001$) (Fig. 2D). Taken together these findings indicate that *Depdc5* loss in our neuron-specific conditional mouse model leads to macrocephaly and increased neuron size, which are common features of models with mTORC1 hyperactivity (Switon et al., 2017).

3.4. Depdc5cc+ mice have dysplastic neurons

Dysplastic neurons are often seen in models of mTOR hyperactivity and have been identified in humans with *DEPDC5* variants (D'Gama et al., 2015b; Scheffer et al., 2014). Dysplastic neurons exhibit cytoskeleton abnormalities such as abnormal cytoplasmic accumulation of argyrophilic fibrils and increased expression of neurofilament proteins visualized by SMI 311 staining (Tassi et al., 2002). Coronal brain sections from control mice exhibited minimal SMI 311 staining limited to sparse III, V, and nonpyramidal layer VI neurons with projections aligned toward the cortical surface as expected (Ulfig et al., 1998) (Fig. 2E, top). In contrast, *Depdc5*cc+ cortical tissue exhibited strong SMI 311 staining throughout the cortex (Fig. 2D, bottom). Many SMI 311-positive layer V neurons in *Depdc5*cc+ mice had clear pyramidal morphology, but dendritic arbors were thicker, and projections appeared disorganized with abnormal orientation (Fig. 2E, bottom right).

3.5. mTOR hyperactivation in Depdc5cc+ neurons

Abnormal mTOR activity underlies many aspects of abnormal cortical development including dysplastic neurons within focal cortical dysplasia (Barkovich et al., 2015). A reliable measure of mTORC1 activity is increased phosphorylation of downstream ribosomal S6 (p-S6 on Ser240/244). We found p-S6 staining to be significantly increased in SMI 311-positive neurons in *Depdc5*cc+ mice compared to controls (Fig. 2E). Our findings are thus consistent with those in *Depdc5*+/− rats (Marsan et al., 2016) and humans with FCDs and *DEPDC5* variants (Scerri et al., 2015), both of which show evidence of increased p-S6 staining in dysplastic neurons.

We performed an evaluation of the cellular specificity of *Depdc5* loss on mTORC1 activation. We assessed the extent of p-S6 staining in neurons, astrocytes, and oligodendrocytes using the markers NeuN, GFAP, and Olig2, respectively. Relatively sparse and weak p-S6 staining was seen in normal-appearing neurons throughout the cortex of control mice (Fig. 3A–C). *Depdc5*cc+ cortical sections demonstrated intense p-S6 staining colocalized with NeuN-positive neurons throughout the cortical layers (Fig. 3D–F). These data indicate *Depdc5* loss in cortical neurons results in increased neuronal soma size and mTORC1 hyperactivation.

We evaluated other brain regions to determine if increased p-S6-stained NeuN-positive neurons were isolated to the cortex of *Depdc5*cc + mice. Increased p-S6 expression was seen throughout the hippocampus of *Depdc5*cc+ mice compared to littermate controls. A fraction of CA1 pyramidal neurons highly expressed p-S6, and many of these neurons were ectopically placed in the stratum oriens (Fig. 3J–L arrows, controls G-I). Nearly all neurons in the CA3 had increased p-S6 staining [Fig. 3, *Depdc5*cc+ (P-R), control (M-O)], and similar to CA1 there was an increase in enlarged ectopic neurons in the *Depdc5*cc+ CA3 hippocampus (Fig. 3L arrows). The dentate gyrus showed increased p-S6 staining in the granular cell layer and the hilum of *Depdc5*cc+ hippocampus compared to controls [Fig. 3, *Depdc5*cc+ (V-X), control (S-U)]. We also observed enlarged, strongly p-S6-positive neurons in other brain regions including the thalamus and amygdala (Supplemental Fig. 1), but not in the caudate and putamen due to relatively sparse Cre expression in the striatum, as previously shown (Yamasaki et al., 2017).These findings strongly indicate that *Depdc5* loss in neurons throughout the majority of the brain results in mTORC1 hyperactivation.

Western blot analyses of cortical lysates were performed to assess semi-quantitively mTOR activation in adult *Depdc5*cc+ mice. We confirmed a 4.8-fold increase ($p < 0.001$) in p-S6 in *Depdc5*cc+ cortical lysates compared to control lysates after normalizing to total S6 levels and alpha-tubulin as a loading control (Fig. 4). Total S6 levels were not significantly changed across genotypes. Decreased AKT phosphorylation (pAKT on Ser473) is expected from feedback signaling by hyperactive mTORC1 and has been reported in *Tsc* models (Meikle et al., 2008). We found a similar reduction of pAKT levels in *Depdc5*cc+ cortical lysates (0.62 ± 0.1 of controls; $p < 0.05$). No changes in TSC1 or TSC2 protein levels were seen, which indicates alterations in mTORC1 activity are not due to reductions in TSC1/TSC2 complex rather the loss of DEPDC5 regulation.

3.6. Reactive astrogliosis in Depdc5cc+ mice

Double labeling for p-S6 and glial markers was performed. There was no colocalization of p-S6 and GFAP staining for astrocytes in *Depdc5*cc+ cortex (Fig. 5D–F). Interestingly, increased GFAP staining and evidence of reactive astrogliosis was present in *Depdc5*cc+ cortical sections (Fig. 5D–F) and was absent in control sections (Fig. 5A–C). Quantification by western blot revealed an increase in GFAP expression in *Depdc5*cc+ cortical lysate compared to controls (Fig. 5G; $p < 0.05$). We assessed for oligodendrocytes by Olig2 staining, and found no colocalization with p-S6 staining in the white or grey matter (Supplemental Fig. 2). Taken together, these data indicate that *Depdc5*cc+ mice have evidence of reactive gliosis, but the increased mTOR activation is specific to neurons.

3.7. Electrophysiologic effects in Depdc5cc+ mice

Video-EEG was recorded by wireless telemetry from a total of 7 *Depdc5*cc+ and 5 littermate control mice. Eight mice were recorded for 60 h of which 2 control and 2 *Depdc5*cc+ mice were 65 days of age, and 1 control and 3 *Depdc5*cc+ mice were between 96 and 115 days old. We also evaluated longer-term recordings in 2 control and 2 *Depdc5*cc+ mice for a total of 10 recording days in mice between 89 and 115 days old. Despite witnessing three *Depdc5*cc+ mice having clear clinical seizures, including a terminal GTC seizure, we did not capture an electroclinical seizure in the 7 mice recorded on video-EEG. All mice had an expected 4–6 Hz background activity at rest with appropriate reactivity to salient stimuli. Rare and short spike trains were seen in *Depdc5*cc+ and control mice (Fig. 6A). Spike trains in *Depdc5*cc+ mice were not sufficiently sustained to qualify as electrographic seizures (Rensing et al., 2012). Similar to *Depdc5*+/− rats, the *Depdc5*cc+ mice did not exhibit significantly different interictal activity compared to control mice (Marsan et al., 2016). EEG frequency bands analyzed over a 1 h period during the day and at night showed no significant

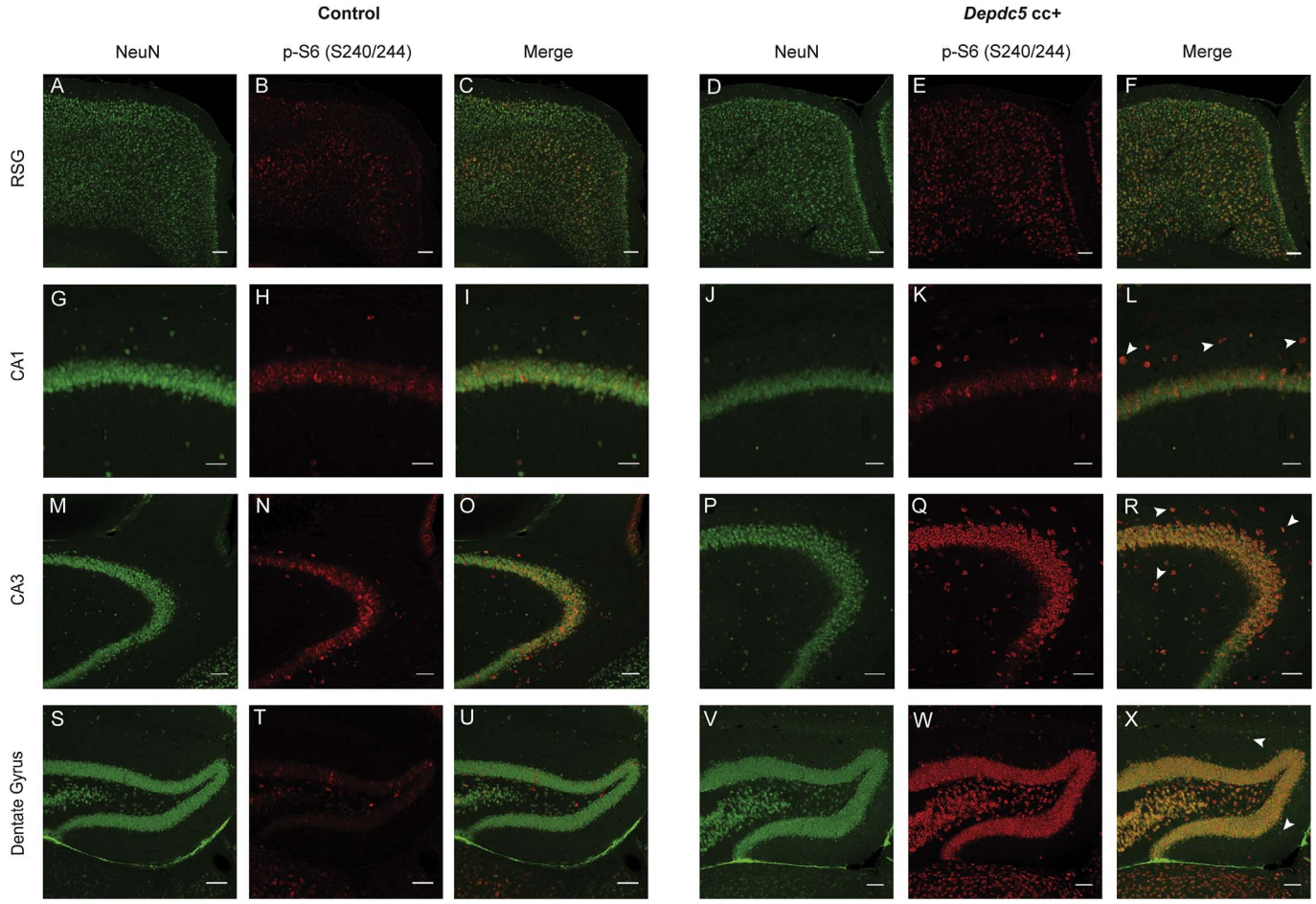

Fig. 3. Widespread architectural abnormalities and evidence of mTORC1 hyperactivation in adult conditional neuron-specific *Depdc5* knockout (*Depdc5*cc+) mice. A–F: Increased p-S6 expression in NeuN + neurons throughout the RSG region of the motor cortex of *Depdc5*cc+ brains (D–F) compared to controls (A–C). G–L: Occasional large p-S6 + neurons within the CA1 pyramidal cell layer of the hippocampus of *Depdc5*cc+ mice (J–L) and also ectopically in the stratum oriens (L; arrowheads). M–R: In the CA3 region of the hippocampus, nearly all neurons are p-S6 + including those outside the pyramidal cell layer (arrowheads) in *Depdc5*cc+ mice (P–R). S–X: In the dentate gyrus, robust p-S6 positive neurons in the granule cell layer and hilus of *Depdc5*cc+ mice (V–X) with a few ectopic neurons (arrowheads). Sections from *Depdc5*cc+ (n = 4) and control (n = 3) brains. Scale bars: 100 μm.

difference in power in individual frequency bands, or power ratio frequencies across genotypes (data not shown).

We then tested whether *Depdc5*cc+ mice have a lowered seizure threshold when challenged with the proconvulsant PTZ while being recorded with video-EEG. After PTZ injection, mice exhibited various clinical epileptic stages from behavioral arrest to myoclonic jerking to GTC seizures. The representative traces show the gradual progression of control (Fig. 6B, top) and *Depdc5*cc+ (Fig. 6B, bottom) mice EEG into a GTC (Fig. 6B, insets) after PTZ injection. *Depdc5*cc+ mice have a significantly shorter latency to GTC seizures after PTZ administration ($p < 0.05$) (Fig. 6C). There was no difference in total GTC seizure duration between the genotypes. After a GTC seizure, *Depdc5*cc+ mice display shorter duration of postictal baseline suppression before myoclonic seizures (Fig. 6B). Sixty-three percent ($n = 5/8$) of *Depdc5*cc+ mice died due to PTZ-induced seizures compared to 9% ($n = 1/11$) of controls ($p < 0.05$) (Fig. 6D). Despite having a relatively normal interictal EEG pattern, these data indicate *Depdc5*cc+ mice have lowered seizure threshold and increased rate of seizure-related death.

4. Discussion

We present the first evidence of an animal model of *DEPDC5*-related epilepsy that recapitulates many features of the human conditions associated with this important epilepsy- and malformation-related gene. Humans with heterozygous loss-of-function *DEPDC5* variants exhibit epilepsy with or without developmental cortical malformations. Histopathology from resected tissue from an individual with a pathogenic *DEPDC5* variant has been reported to show increased mTORC1 activity by p-S6 staining in cytomegalic neurons (Scerri et al., 2015). Familial *DEPDC5*-related epilepsy penetrance is variable and incomplete (Dibbens et al., 2013; Ishida et al., 2013; Scheffer et al., 2014), raising the question of whether a second somatic variant may be required to create loss of function in a localized region and thus focal epilepsy. Given published evidence that a "two-hit" functional knockout of *DEPDC5* may underlie the human condition (Baulac et al., 2015), we created a neuron-specific *Depdc5* knockout mouse model to analyze *in vivo* the effects of loss of function of DEPDC5 in the brain.

We utilized a *Depdc5* floxed allele combined with a *Synapsin I* promotor-driven Cre allele to eliminate Depdc5 in the majority of neurons beginning at E13. This resulted in excision of exon 5 from the *Depdc5* gene exclusively in the brain. Despite the lack of availability of reliable DEPDC5 antibodies for mouse tissue, we demonstrated brain-specific loss of full-length *Depdc5* mRNA by RT-PCR. Taken together, our data provide convincing evidence of Cre-mediated excision of *Depdc5* exon 5, reduced full-length *Depdc5* transcript, and an expected phenotype similar to humans with *DEPDC5* variants and other mTORopathies (Scheffer et al., 2014).

*Depdc5*cc+ mice exhibit many features consistent with mTORopathies (Lipton and Sahin, 2014). *Depdc5*cc+ mice have late onset poor weight gain similar to the hypomorphic *Tsc2*cc+ ($Tsc2^{cc}$-Syn^{Cre+}) mice, but less severe than *Tsc1*cc+ ($Tsc1^{cc}$-Syn^{Cre+}) that have marked weight loss and wasting syndrome. Weight reduction was only

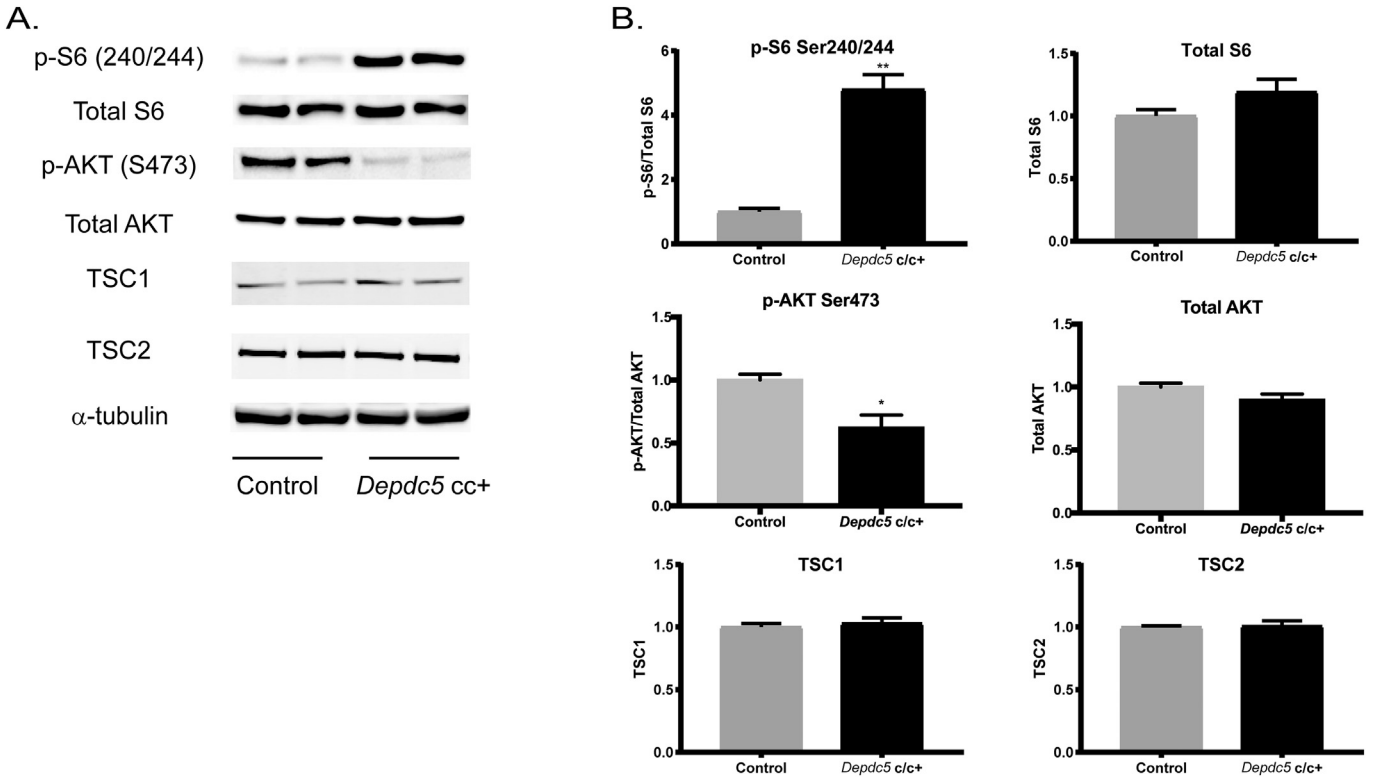

Fig. 4. mTORC1-signaling is increased in conditional neuron-specific *Depdc5* knockout (*Depdc5*cc+) cortical lysates. (A) Immunoblots and (B) quantitative analysis of cortical brain lysates from adult (92–122 day old) *Depdc5*cc+ and littermate control mice demonstrate altered regulation of mTORC1 by increased p-S6(S240/244) and decreased p–AKT(S473) in *Depdc5*cc+ brains, which is independent of TSC1 and TSC2. Analysis from ≥ 3 samples per genotype. Expression of levels were normalized to alpha-tubulin, and p-S6(S240/244) and p–AKT(S473) were normalized to total levels of S6 and AKT, respectively. All ratios for the control samples are normalized to 1 with mean ± SEM. *$p < 0.05$; **p < 0.01 (Student's *t*-test).

noted in male *Depdc5*cc+ mice. The reason for the sex difference is unclear, but prior studies have noted sex-dependent effects of mTORC1 on lifespan and longevity (Selman et al., 2009). The neurological phenotype, however, was seen in both sexes, and no differences among subsequent analysis were seen. *Depdc5*cc+ mice displayed mild hind limb clasping behavior in aged mice that correlates with neurological dysfunction. These findings are similar to but milder than the TSC models (Meikle et al., 2007; Yuan et al., 2012). The brain pathology of *Depdc5*cc+ mice demonstrated increased brain weight and larger neuronal size, which are typical of mTORopathies (Winden et al., 2015). Neuronal density was decreased in the deeper cortical layers of *Depdc5*cc+ mice, consistent with *Tsc1-Nestin*$^{Cre+}$ mice (Anderl et al., 2011). Importantly, we found evidence of dysplastic cortical neurons of *Depdc5*cc+ mice. Similar dysplastic neurons are also found in developmental brain malformations of patients with *DEPDC5* variants (Scerri et al., 2015).

We demonstrate that neuronal *Depdc5* loss results in mTOR hyperactivation restricted to neurons as measured by downstream p-S6 in the *Depdc5*cc+ mice. Our results are consistent with those of previous studies, with increased p-S6 with DEPDC5 loss both *in vivo* (Marsan et al., 2016) and *in vitro* (Bar-Peled et al., 2013), which confirm that DEPDC5 loss results in increased mTORC1 activity. Interestingly, *Depdc5*cc+ cortical lysates show a reduction in AKT activity as measured by decreased AKT Ser473 phosphorylation. TSC knockout models also exhibit reduction in pAKT levels (Yuan et al., 2012). Decreased pAKT after TSC2 loss is thought to be mediated by either feedback mechanisms or direct effects on mTOR2 (Um et al., 2004). Our data indicate common downstream effects between TSC and GATOR mediated mTOR regulation, yet further studies are needed to delineate similarities and differences between these pathways. Taken together, our results demonstrating DEPDC5 regulation of mTOR corroborates prior *in vivo* and *in vitro* data, but, importantly, add the first surviving model to study the role of DEPDC5 *in vivo*.

Neuronal *Depdc5* loss results in astrogliosis in our neuron-specific model. Astrogliosis is common in epilepsy and is implicated in promoting epileptogenesis (Coulter and Steinhauser, 2015). mTORC1 may play a role in reactive astrogliosis formation after seizures, and inhibition of mTOR by rapamycin attenuates seizure-induced astrocyte injury (Guo et al., 2017). *Depdc5cc+* mice did not show constitutively elevated mTOR activation in astrocytes as measured by p-S6 staining. These results suggest that the astrogliosis may be a result of dysfunctional neural activity or seizures related to loss of *Depdc5* in neurons, which has been demonstrated in other mTORopathy models (Switon et al., 2017). It is also possible that neuronal mTOR activity interacts with neighboring astrocytes *via* a secreted/extracellular molecular as we have shown to occur between neurons and oligodendrocytes (Ercan et al., 2017). Our identification of astrogliosis in *Depdc5cc+* mice provide a foundation for future studies to uncover the mechanism of astrogliosis after DEPDC5 loss.

The background EEG pattern in *Depdc5*cc+ mice was relatively normal, which is not inconsistent with the observations that many individuals with focal epilepsy may have a normal interictal EEG (Pillai and Sperling, 2006). Although we did not capture seizures on EEG, we witnessed three mice have clinical seizures, one immediately precipitating death of the animal and mimicking the human phenomenon of seizure-related death that falls under the category of SUDEP. It is possible that EEG recording even closer to the time of death may exhibit interictal abnormalities. Other mTOR-related conditional knockout mice models such as *Tsc1cc+* and *Tsc2cc+* mice exhibit terminal seizures (Meikle et al., 2007; Yuan et al., 2012), therefore we suspect that terminal seizure events were a major cause of death of *Depdc5*cc+ mice as well.

Interestingly, the witnessed seizures in *Depdc5*cc+ mice that did not result in death were not GTC seizures but rather prolonged periods (up to 1 min) of unresponsive tonic freezing. The low rate of spontaneous

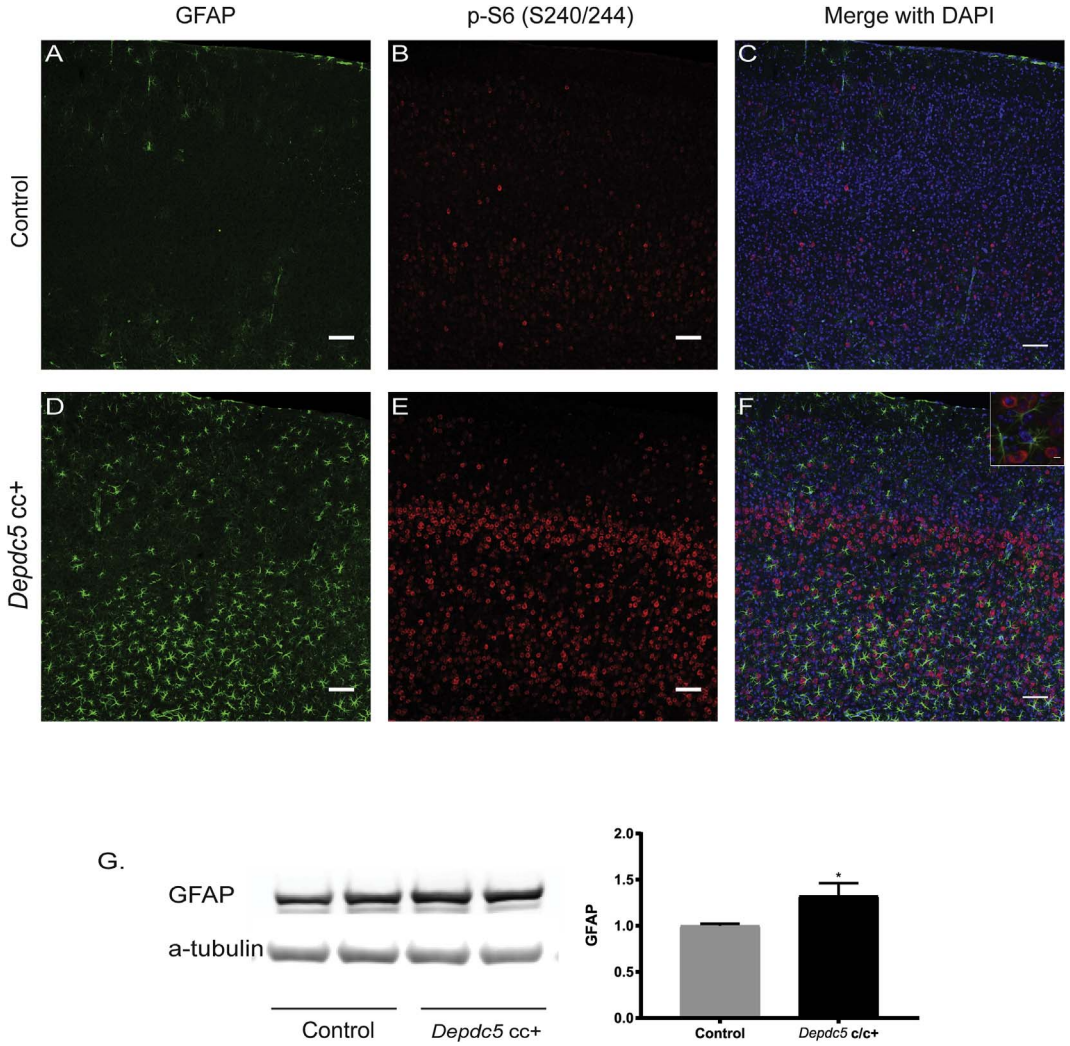

Fig. 5. Evidence of reactive astrogliosis in conditional neuron-specific *Depdc5* knockout (*Depdc5*cc+) mice. Astrogliosis was absent in control cortical sections (n = 3 mice) (Fig. 5A–C) and present in adult *Depdc5*cc+ cortical sections (n = 4 mice) (Fig. 5D–F). Scale bars: 50 μm. (F) Inset demonstrates lack of GFAP and p-S6 colocalization, scale bar = 10 μm. (G) Immunoblots and quantitative analysis of cortical brain lysates for GFAP from adult *Depdc5*cc+ and littermate control mice (n = 8 per genotype). Expression of levels were normalized to alpha-tubulin and control samples are normalized to 1 with mean ± SEM. $^{*}p < 0.05$; $^{**}p < 0.01$ (Student's t-test).

seizures in our model (3 of 43 *Depdc5*cc+ mice), with 0/7 mice recorded on video-EEG displaying seizures, led us to evaluate propensity to seizure using a PTZ-induced seizure paradigm that clearly demonstrated lowered seizure threshold in our model. These results are comparable to those reported in a mouse model deficient in SZT2, part of the KICSTOR complex upstream of DEPDC5 (Peng et al., 2017; Wolfson et al., 2017), which also have a lowered seizure threshold to PTZ but do not have spontaneous or stress-induced seizures (Frankel et al., 2009).

TSC models generally have a more severe phenotype with frequent unprovoked seizures (see review (Switon et al., 2017)) compared to our *Depdc5* model or the *Szt2* model (Frankel et al., 2009). DEPDC5 and SZT2 are implicated in mTOR mediated amino acid sensing, which is distinct from the TSC pathway (Saxton and Sabatini, 2017). These data support the hypothesis that these two pathways upstream of mTORC1 have different effects, also supported by the observation that the human phenotypes where *DEPDC5*-related epilepsy is often less severe and more responsive to medication as compared to TSC (Scheffer et al., 2014). We hypothesize that the less severe phenotype with DEPDC5 loss is a result of the intact feedback inhibition of mTORC1 through mTORC2, AKT, and TSC (Um et al., 2004). Further studies directly comparing *Tsc* and *Depdc5* animal models may elucidate the phenotypic differences across the mTORopathies.

We also demonstrated increased death related to seizures in *Depdc5cc+* mice compared to controls, in one of the two animals with spontaneous seizures and in the animals with PTZ-induced seizures. SUDEP is an important cause of mortality related in particular to patients with epilepsy who have pathogenic *DEPDC5* variants (Bagnall et al., 2016; Nascimento et al., 2015; Weckhuysen et al., 2016) and to TSC patients (Amin et al., 2017). The pathophysiology and molecular underpinnings of SUDEP are unknown, including the specific mechanisms related to these genes. Given the mortality of otherwise healthy-appearing *Depdc5*cc+ mice, further characterization of the cardiopulmonary features and electrophysiological characteristics preceding the death of *Depdc5*cc+ mice will provide a potential model to understand the pathophysiology of SUDEP.

5. Conclusions

We demonstrate in a neuron-specific conditional knockout mouse model that *Depdc5* loss of function plays a critical role in epileptogenesis and brain development. *Depdc5*cc+ mice display a propensity to proconvulsant-induced and rare spontaneous behavioral seizures, sometimes associated with increased mortality. We thus report the first animal model of *DEPDC5*-related epilepsy and present a model that may be studied in future to elucidate the currently elusive mechanisms of SUDEP. Thus, our *Depdc5*cc+ model recapitulates many of the features

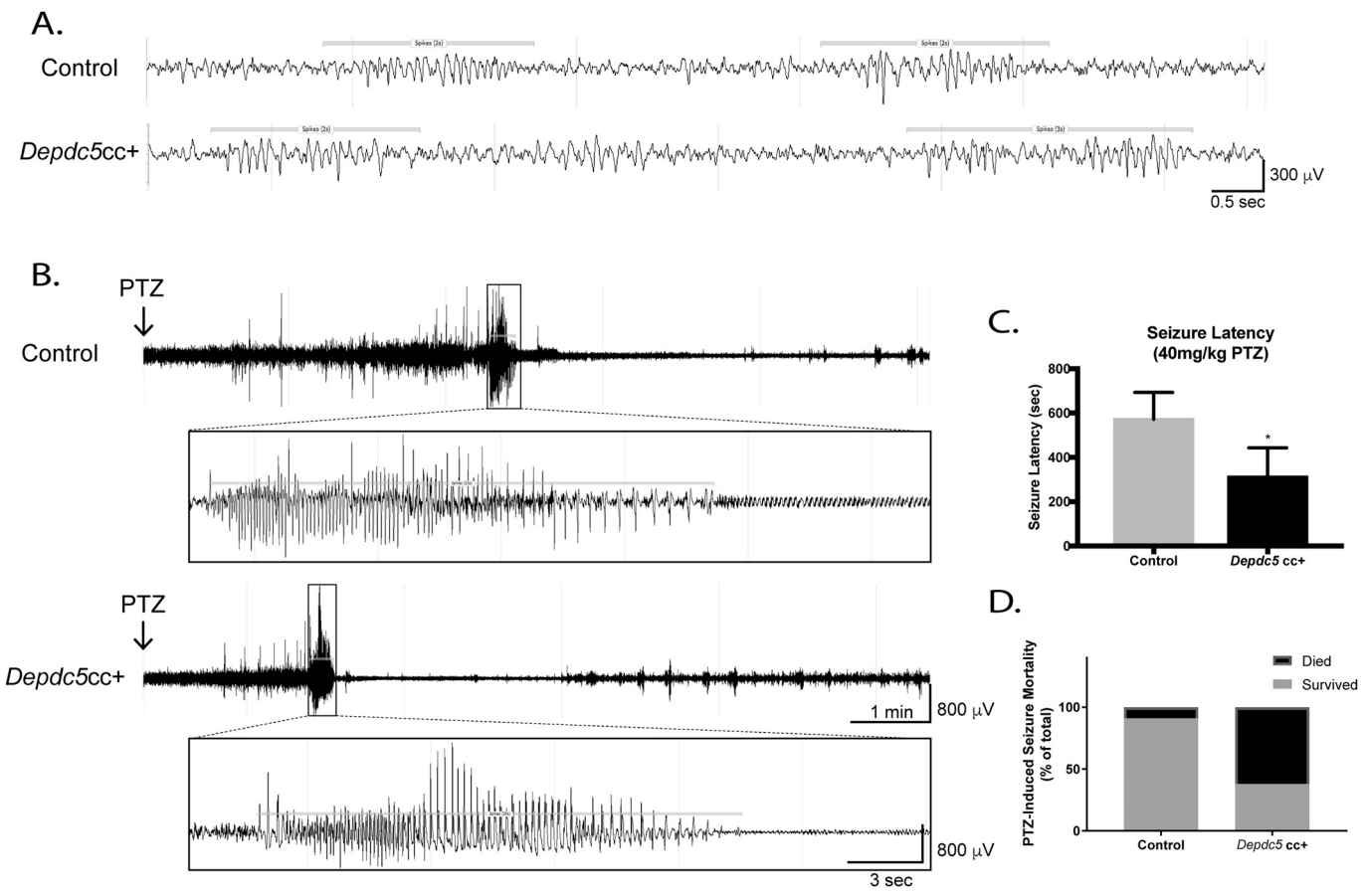

Fig. 6. Electrophysiologic defects are evident in conditional neuron-specific *Depdc5* knockout (*Depdc5*cc+) mice. (A) Representative baseline EEG data from control and *Depdc5*cc+ mice demonstrates 2-s spike trains (horizontal bars; a normal rodent EEG finding) intermixed with a normal background EEG pattern. (B) Representative EEG tracings after PTZ injection demonstrate a shorter latency to GTC seizures in *Depdc5*cc+ mice. Clinical seizure onset corresponds to left box margin. (C) *Depdc5*cc+ mice (n = 8) have a shorter latency to GTC seizures after 40 mg/kg PTZ administration compared to controls ($n = 11$). $p < 0.05$, one-tailed Mann-Whitney test. (D) Increased mortality of *Depdc5*cc+ mice (n = 8) compared to controls after 40 mg/kg PTZ, $p < 0.05$ by Chi-Square analysis.

of the human patients with *DEPDC5* pathogenic variants as well as other models of mTORopathies. Further, *Depdc5*cc+ mice have increased brain size, increased cortical thickness, and neuropathological abnormalities, including larger neurons and dysplastic neurons similar to those seen in focal cortical dysplasia tissue in humans. We demonstrate that these findings are due to increased mTORC1 activation specifically in neurons by isolated neuronal p-S6 staining. Despite restriction of mTORC1 activation to neurons, *Depdc5*cc+ brains have evidence of reactive astrocytes, suggesting non-cell-autonomous effects of mTORC1 hyperactivation in neurons. The precise mechanisms by which this neuron-specific mTORC1-related pathology leads to epilepsy require additional study. The *Depdc5*cc+ mouse will provide an essential model to develop and test mTORC1 inhibitors and targeted novel therapeutics.

Acknowledgments

We would like to thank the IDDRC Cellular Imaging Core at Boston Children's Hospital and Dr. Anthony Hill for imaging assistance, Samantha Murphy for aid in generating mice, Samantha Schaeffer for animal breeding, Dr. Alessia Di Nardo for antibodies, Allison Mazzella for technical assistance, and the Experimental Neurophysiology Core at Boston Children's Hospital.

Funding

This work was supported by the NIH 2R25NS070682-07 (CJY) and U54HD090255 (MS), and the Translational Research Program at Boston Children's Hospital (AP).

Appendix A. Supplementary data

Supplementary data to this article can be found online at https://doi.org/10.1016/j.nbd.2017.12.010.

References

Amin, S., et al., 2017. Causes of mortality in individuals with tuberous sclerosis complex. Dev. Med. Child Neurol. 59, 612–617.
Anderl, S., et al., 2011. Therapeutic value of prenatal rapamycin treatment in a mouse brain model of tuberous sclerosis complex. Hum. Mol. Genet. 20, 4597–4604.
Bagnall, R.D., et al., 2016. Exome-based analysis of cardiac arrhythmia, respiratory control, and epilepsy genes in sudden unexpected death in epilepsy. Ann. Neurol. 79, 522–534.
Barkovich, A.J., et al., 2015. Malformations of cortical development and epilepsy. Cold Spring Harb. Perspect. Med. 5, a022392.
Bar-Peled, L., et al., 2013. A tumor suppressor complex with GAP activity for the rag GTPases that signal amino acid sufficiency to mTORC1. Science 340, 1100–1106.
Baulac, S., et al., 2015. Familial focal epilepsy with focal cortical dysplasia due to DEPDC5 mutations. Ann. Neurol. 77, 675–683.
Carvill, G.L., et al., 2015. Epileptic spasms are a feature of DEPDC5 mTORopathy. Neurol Genet. 1, e17.

Coulter, D.A., Steinhauser, C., 2015. Role of astrocytes in epilepsy. Cold Spring Harb. Perspect. Med. 5, a022434.
D'Gama, A.M., et al., 2015a. Mammalian target of rapamycin pathway mutations cause hemimegalencephaly and focal cortical dysplasia. Ann. Neurol. 77, 720–725.
D'Gama, A.M., et al., 2015b. Mammalian target of rapamycin pathway mutations cause hemimegalencephaly and focal cortical dysplasia. Ann. Neurol. 77, 720–725.
Dhamne, S.C., et al., 2015. Acute seizure suppression by transcranial direct current stimulation in rats. Ann. Clin. Transl. Neurol. 2, 843–856.
Dhamne, S.C., et al., 2017. Replicable in vivo physiological and behavioral phenotypes of the Shank3B null mutant mouse model of autism. Mol. Autism 8, 26.
Di Cristofano, A., et al., 1998. Pten is essential for embryonic development and tumour suppression. Nat. Genet. 19, 348–355.
Dibbens, L.M., et al., 2013. Mutations in DEPDC5 cause familial focal epilepsy with variable foci. Nat. Genet. 45, 546–551.
Dickinson, M.E., et al., 2016. High-throughput discovery of novel developmental phenotypes. Nature 537, 508–514.
Epik4K consortium, Epilepsy Phenome/Genome Project, 2017. Ultra-rare genetic variation in common epilepsies: a case-control sequencing study. Lancet Neurol. 16, 135–143.
Ercan, E., et al., 2017. Neuronal CTGF/CCN2 negatively regulates myelination in a mouse model of tuberous sclerosis complex. J. Exp. Med. 214, 681–697.
Frankel, W.N., et al., 2009. Szt2, a novel gene for seizure threshold in mice. Genes Brain Behav. 8, 568–576.
Guo, D., et al., 2017. Rapamycin attenuates acute seizure-induced astrocyte injury in mice in vivo. Sci. Rep. 7, 2867.
Han, J.M., Sahin, M., 2011. TSC1/TSC2 signaling in the CNS. FEBS Lett. 585, 973–980.
Ishida, S., et al., 2013. Mutations of DEPDC5 cause autosomal dominant focal epilepsies. Nat. Genet. 45, 552–555.
Lal, D., et al., 2014. DEPDC5 mutations in genetic focal epilepsies of childhood. Ann. Neurol. 75, 788–792.
Lipton, J.O., Sahin, M., 2014. The neurology of mTOR. Neuron 84, 275–291.
Marsan, E., et al., 2016. Depdc5 knockout rat: a novel model of mTORopathy. Neurobiol. Dis. 89, 180–189.
Meikle, L., et al., 2007. A mouse model of tuberous sclerosis: neuronal loss of Tsc1 causes dysplastic and ectopic neurons, reduced myelination, seizure activity, and limited survival. J. Neurosci. 27, 5546–5558.
Meikle, L., et al., 2008. Response of a neuronal model of tuberous sclerosis to mammalian target of rapamycin (mTOR) inhibitors: effects on mTORC1 and Akt signaling lead to improved survival and function. J. Neurosci. 28, 5422–5432.
Nascimento, F.A., et al., 2015. Two definite cases of sudden unexpected death in epilepsy in a family with a DEPDC5 mutation. Neurol Genet. 1, e28.
Peng, M., et al., 2017. SZT2 dictates GATOR control of mTORC1 signalling. Nature 543, 433–437.
Picard, F., et al., 2014. DEPDC5 mutations in families presenting as autosomal dominant nocturnal frontal lobe epilepsy. Neurology 82, 2101–2106.
Pillai, J., Sperling, M.R., 2006. Interictal EEG and the diagnosis of epilepsy. Epilepsia 47 (Suppl. 1), 14–22.
Rensing, N.R., et al., 2012. Video-EEG monitoring methods for characterizing rodent models of tuberous sclerosis and epilepsy. Methods Mol. Biol. 821, 373–391.
Ricos, M.G., et al., 2016. Mutations in the mammalian target of rapamycin pathway regulators NPRL2 and NPRL3 cause focal epilepsy. Ann. Neurol. 79, 120–131.
Saxton, R.A., Sabatini, D.M., 2017. mTOR signaling in growth, metabolism, and disease. Cell 168, 960–976.
Scerri, T., et al., 2015. Familial cortical dysplasia type IIA caused by a germline mutation in DEPDC5. Ann. Clin. Transl. Neurol. 2, 575–580.
Scheffer, I.E., et al., 2014. Mutations in mammalian target of rapamycin regulator DEPDC5 cause focal epilepsy with brain malformations. Ann. Neurol. 75, 782–787.
Selman, C., et al., 2009. Ribosomal protein S6 kinase 1 signaling regulates mammalian life span. Science 326, 140–144.
Shimobayashi, M., Hall, M.N., 2016. Multiple amino acid sensing inputs to mTORC1. Cell Res. 26, 7–20.
Switon, K., et al., 2017. Molecular neurobiology of mTOR. Neuroscience 341, 112–153.
Tassi, L., et al., 2002. Focal cortical dysplasia: neuropathological subtypes, EEG, neuroimaging and surgical outcome. Brain 125, 1719–1732.
Ulfig, N., et al., 1998. Monoclonal antibodies SMI 311 and SMI 312 as tools to investigate the maturation of nerve cells and axonal patterns in human fetal brain. Cell Tissue Res. 291, 433–443.
Um, S.H., et al., 2004. Absence of S6K1 protects against age- and diet-induced obesity while enhancing insulin sensitivity. Nature 431, 200–205.
Weckhuysen, S., et al., 2016. Involvement of GATOR complex genes in familial focal epilepsies and focal cortical dysplasia. Epilepsia 57, 994–1003.
Winden, K.D., et al., 2015. Megalencephaly and macrocephaly. Semin. Neurol. 35, 277–287.
Wolfson, R.L., et al., 2017. KICSTOR recruits GATOR1 to the lysosome and is necessary for nutrients to regulate mTORC1. Nature 543, 438–442.
Yamasaki, T., et al., 2017. Age-dependent motor dysfunction due to neuron-specific disruption of stress-activated protein kinase MKK7. Sci. Rep. 7, 7348.
Yuan, E., et al., 2012. Graded loss of tuberin in an allelic series of brain models of TSC correlates with survival, and biochemical, histological and behavioral features. Hum. Mol. Genet. 21, 4286–4300.
Zhu, Y., et al., 2001. Ablation of NF1 function in neurons induces abnormal development of cerebral cortex and reactive gliosis in the brain. Genes Dev. 15, 859–876.